Atmos. Chem. Phys. Discuss., 12, 15837–15881, 2012
www.atmos-chem-phys-discuss.net/12/15837/2012/
doi:10.5194/acpd-12-15837-2012

Atmospheric Chemistry and Physics Discussions

Idealized WRF model sensitivity simulations of sea breeze types and their effects on offshore windfields

C. J. Steele[1], S. R. Dorling[1,2], R. von Glasow[1], and J. Bacon[2]

[1]School of Environmental Sciences, University of East Anglia, Norwich, Norfolk, NR4 7TJ, UK
[2]Weatherquest Ltd, University of East Anglia, Norwich, Norfolk, NR4 7TJ, UK

Received: 26 April 2012 – Accepted: 30 May 2012 – Published: 26 June 2012

Correspondence to: C. J. Steele (christopher.steele@uea.ac.uk)

Published by Copernicus Publications on behalf of the European Geosciences Union.

Abstract

The behaviour and characteristics of the marine component of sea breeze cells have received little attention relative to their onshore counterparts. Yet there is a growing interest and dependence on the offshore wind climate from, for example, a wind energy perspective. Using idealized model experiments, we investigate the sea breeze circulation at scales which approximate to those of the Southern North Sea, a region of major ongoing offshore wind farm development. We also contrast the scales and characteristics of the *pure* and the little known *corkscrew* and *backdoor* sea breeze types, where the type is pre-defined by the orientation of the synoptic scale flow relative to the shoreline. We find, crucially, that *pure* sea breezes, in contrast to *corkscrew* and *backdoor* types, can lead to substantial wind speed reductions offshore and that the addition of a second eastern coastline emphasises this effect through generation of offshore "calm zones". The offshore extent of all sea breeze types is found to be sensitive to both the influence of Coriolis acceleration and to the boundary layer scheme selected. These extents range, for example for a *pure* sea breeze produced in a $2\,m\,s^{-1}$ offshore gradient wind, from 10 km to 40 km between the Mellor-Yamada-Nakanishi-Niino and the Yonsei State University schemes, respectively. The *corkscrew* type restricts the development of a *backdoor* sea breeze on the eastern coast and is also capable of traversing a 100 km offshore domain even under high gradient wind speed ($>15\,m\,s^{-1}$) conditions. Realistic variations in sea surface skin temperature during the sea breeze season do not significantly affect the circulation, suggesting that a thermal contrast is only needed as a precondition to the development of the sea breeze. We highlight how sea breeze impacts on circulation need to be considered in order to improve the accuracy of assessments of the offshore wind energy climate.

ACPD

12, 15837–15881, 2012

1 Introduction

The sea breeze has been documented in historical texts as early as ancient Greece and to date there have been as many as 1300 articles on the subject, making the sea breeze one of the most intensely studied meso-scale meteorological phenomena. Consequently, the structure and physics of the sea breeze onshore are well known, including the features such as Kelvin-Helmholtz instabilities, sea breeze head, and associated frontal components (Simpson, 1994, Fig. 1). By far the largest contributor, accounting for approximately half of the aforementioned literature, are air quality and pollution studies (e.g. Borge et al., 2008; Lee et al., 2011; Fernández-Camacho et al., 2010). Depending on the position and height of the pollution source, the sea breeze can act to either concentrate or disperse pollutants. With a large proportion of the global population living in proximity to a coastline, and the sea breeze representing a significant feature of the seasonal coastal climate, forecasting both the physics and chemistry of these features is consequently of high importance. Furthermore, sea breezes also interact with other thermally induced flows such as with mountain valley winds, with urban heat island circulations and indeed with other sea breeze systems (Clarke et al., 1981; Bianco et al., 2006; Tsunematsu et al., 2009). They have even been associated with severe localized flooding (Brian et al., 2005).

Since a sea breeze is able to form on any coastline where the land-sea temperature gradient is sufficiently strong to overcome the synoptic pressure gradient, sea breeze study locations vary tremendously. Studies commonly appear in the literature focusing on Spain (e.g. Azorin-Molina et al., 2011a), Japan (e.g. Tsunematsu et al., 2009), Australia (e.g. Clarke, 1989), Sardinia (e.g. Furberg et al., 2002) Finland (e.g. Savijarvi and Alestalo, 1988), Greece (e.g. Papanastasiou et al., 2010) and the United States of America (e.g. Challa et al., 2009).

With the myriad of possible motivations, interactions and locations to study sea breezes, it is easy to explain the number of articles and thorough reviews can be found in Abbs and Physick (1992), in Miller et al. (2003) and in Crosman and Horel (2010)

ACPD
12, 15837–15881, 2012

for additional information. However, not withstanding this extensive literature on sea breeze characteristics, interactions and study locations, there is a general absence of studies focusing on the marine component despite being of great relevance to the developing offshore wind energy industry (Crosman and Horel, 2010). Also apparent is a general lack of attention given to the different sea breeze types, which are classified in accordance with the orientation of the gradient wind, adding further complexity to the task of forecasting (Hoddinott, 2009; Miller et al., 2003). Both of these aspects are investigated further here.

Originally from nautical origins, the types of sea breeze are known in the Northern Hemisphere as:

- *Pure* – sea breeze circulation with largest gradient wind component perpendicular to the coast and in the offshore direction (Fig. 1).
- *Corkscrew* – sea breeze with largest gradient wind component parallel to the coast and land surface to the left (Fig. 2).
- *Backdoor* – sea breeze with largest gradient wind component parallel to the coast and land surface to the right (Fig. 2).

The *pure* type is the most intensely studied type of sea breeze (Crosman and Horel, 2010; Finkele, 1998; Azorin-Molina and Chen, 2009). Primarily, this is due to the ease of creation of an identification method relying on the winds reversing from offshore to onshore (e.g. Azorin-Molina et al., 2011b). Diagnosing the offshore extent of a sea breeze is also simpler with the *pure* type, since a distance offshore can be defined where the wind speed exceeds a particular threshold (Arritt, 1989).

When considering along-shore gradient winds and the subsequent generation of *corkscrew* and *backdoor* sea breezes, the Buys-Ballot law and frictional differences must be taken into account (Fig. 2). In the *corkscrew* case, the Buys-Ballot law implies that low pressure is situated over the land surface. This, when combined with frictional differences between land and sea, creates a region of divergence at the coastal boundary that strengthens the sea breeze circulation. Consequently, it could be the case that

ACPD
12, 15837–15881, 2012

a *corkscrew* sea breeze could form with a weaker thermal contrast, relative to the *pure* type, and so this is investigated further here. Conversely the Buys-Ballot law implies that, for the *backdoor* sea breeze, low pressure is situated over the sea and therefore a region of convergence is created at the coast. Consequently, this implies that a stronger thermal contrast is needed between the land and sea to generate this type of sea breeze.

Crosman and Horel (2010) note that there are both a lack of studies focusing on the offshore sea breeze cell component and a deficiency of studies looking at sea breeze sensitivity to the extent of the water body. Indeed, in a review of over 50 yr of sea breeze modelling studies they highlight only two influential papers focusing entirely on the offshore component. In the first study by Arritt (1989), 2- and 3-dimensional model simulations were performed to determine the environmental controls on the offshore extent of sea breezes. Arritt (1989) defined the offshore extent to be the region where onshore wind speeds were greater than $1\,m\,s^{-1}$. Latitude and synoptic forcing were found to have the most significant effect; both higher latitudes and offshore gradient flows greatly reduced the offshore extent. Also, it was determined that if the Sea Surface Temperature (SST) was sufficiently warm to produce a convective boundary layer, then the sea breeze was weakened. However, if the water was sufficiently cold to produce a stable surface layer, any further cooling did not have an additional effect.

More recently, in the second study, Finkele (1998) used a 3-dimensional hydrostatic model to ascertain offshore propagation speeds, with the help of airborne measurements. Principally, in contrast to Arritt (1989), it was found that the offshore extent was similar for both light ($2.5\,m\,s^{-1}$) and moderate ($5\,m\,s^{-1}$) offshore geostrophic wind conditions. The propagation speeds for both onshore and offshore development were non-uniform at these wind speeds. Finkele (1998) also suggested that the onshore extent was more sensitive to geostrophic wind speed than the offshore, though it was added that during periods when wind speeds were greater than $7.5\,m\,s^{-1}$ the sea breeze had become entirely detached and so it was no longer possible to confirm. Both studies report, however, that the offshore extent can be several times that of the onshore, and

ACPD
12, 15837–15881, 2012

can reach distances of the order of 100–150 km given appropriate conditions. Potentially, this could be restricted if there were an additional coastline on the opposite side of the sea, similarly generating sea breezes.

Unfortunately, the effect of a second coastline is an important detail that is also under-studied; Savijarvi and Alestalo (1988) addressed this point but, even so, the primary focus remained on the inland component. Their aim was to use a 2-dimensional mesoscale model to simulate sea breezes across a channel 80 km wide with SST, land surface temperature and roughness length variations representative of the Gulf of Finland. Both wind speed and direction were varied to examine the behaviour of the sea breeze in this situation. In particular, Savijarvi and Alestalo (1988) note that the sea breeze was insensitive to the strength of along-shore gradient winds, however offshore winds generated a low level jet along the coast and suppressed sea breeze inland penetration.

There is now a pressing need to progress our understanding of the scale and climatology of the marine component of the sea breeze cell to support the rapidly expanding offshore wind energy industry. Around the coast of Britain, there are currently 15 offshore wind farms, with a further 21 either under construction or in planning (Fig. 3). Such is the scale of the industry that, by 2020, it is planned that offshore wind power will account for 17 % of the total electrical power output of the UK (RenewableUK, 2012). A large proportion of these wind farms are situated in the relatively shallow Southern North Sea between the UK and mainland Europe. The horizontal extent of the North Sea, for example between Gunfleet sands (South East England) and Thornton Bank (Western Netherlands), is approximately 100 km (Fig. 3). Since sea breezes can form under moderate gradient wind speeds, it is entirely plausible that the power produced by these wind farms will be modulated by the sea breeze. It is therefore vital to be able to quantify this potential impact on power output.

With a very limited amount of offshore measurement data available, the few studies that have examined sea breeze marine components have often been restricted to numerical simulations. Here, we perform numerical simulations of idealized sea breezes

ACPD
12, 15837–15881, 2012

using the Weather Research and Forecasting (WRF) model, testing the response to both SST variations, Coriolis forcing and the strength and direction of the gradient wind. Three different boundary layer physics schemes are also tested in order to assess the consistency of results in terms of timing, extent, duration and strength of the sea breeze.

2 Methods

For each simulation, the idealized version of the Weather Research and Forecasting (WRF) model was used, that is, using the full physics equations but with a 2-dimensional model domain (Skamarock and Klemp, 2008). It has been noted by Crosman and Horel (2010) that idealized studies to date overwhelmingly use idealized vertical profiles as initial conditions and so subsequently there is a need to move towards using observations. Here, we used a specific sounding from Herstmonceux radiosonde station in South East England (50.9° N, 0.317° E; Fig. 4). Simpson (1994) note that the most common period for observing sea breezes in the UK is during June, where the land-sea thermal contrast is at a maximum. For this reason the sounding was chosen from the 3 June 2006; a day where sea breeze favouring anticyclonic conditions also dominated the weather of the UK.

2.1 Single coast exploratory experiments

Initially, several single coast simulations were conducted in order to act as a comparison for later dual-coast results. This was also deemed necessary since there has been disagreement in the literature about the sensitivity of the sea breeze offshore extent to gradient flow (Crosman and Horel, 2010).

For each test, the model was initialized at midnight and simulations were run for 24 h, with a time step of 10 s and with output recorded every 15 min. The land use category was selected as *dryland, cropland and pasture* to best represent the Eastern UK. The

ACPD
12, 15837–15881, 2012

model domain was divided so that 100 grid points occupied land and 100 represented sea. The model horizontal resolution was 3 km and 35 vertical layers were distributed so that 8 layers were in the lowest 1 km and the remainder distributed to a height of 15 km. Coriolis acceleration was enabled for a latitude of 52° for these experiments to best represent the Southern North Sea. The initial land and sea skin temperatures were 280 K and 287 K, respectively. Model simulations consisted of varying the along-shore and offshore gradient winds from 2 to 10 $m s^{-1}$ in steps of 2 $m s^{-1}$ so as to generate the different types of sea breeze. The offshore extent for all simulations was defined using the method of Arritt (1989), that is where the strength of the onshore flow breaches 1 $m s^{-1}$. Anything smaller than this threshold is not considered to be part of the sea breeze. A single simulation was also run without gradient winds so that a baseline could be established for comparison with the other sea breeze types. This is referred to as the baseline experiment for which the model physics and settings are described in Table 1.

2.2 Dual coast experiments

The second coastline was added so that a central sea channel occupied the central 99 km of the model domain (Fig. 5). Once again, the land use category was selected as *dryland, cropland* and *pasture* to best represent the UK and mainland Europe. Simulations were run to test the effect of varying gradient wind strengths, Sea Surface Temperature (SST) and Coriolis on three different Planetary Boundary (PBL) schemes; The Yonsei State University (YSU), the Mellor-Yamada-Janjic (MYJ) and the Mellor-Yamada-Nakanishi-Niino (MYNN) schemes (Table 2). SST variations matched those typically experienced in the Southern North Sea during June. Simulations were also carried out with and without Coriolis acceleration for a latitude of 52°, since the effect of Coriolis variations with latitude on the sea breeze is under studied (Crosman and Horel, 2010).

The YSU scheme is a non-local turbulence closure scheme with explicit treatment of the entrainment process (Hong et al., 2006). The scheme includes a parabolic K-mixing

ACPD
12, 15837–15881, 2012

profile for the convective boundary layer and the use of the bulk Richardson number to determine PBL height. The YSU PBL scheme been shown to give a good representation of a sea breeze in previous simulations (Challa et al., 2009). However, in the context of offshore wind energy forecasting, it was indicated by Krogsaeter et al. (2011) that the YSU scheme consistently produces a profile which is excessively neutral offshore, though this was more notable for higher wind speeds. Their study is particularly relevant as Krogsaeter et al. (2011) make use of the FINO 1 platform, located in the Southern North Sea, to verify their PBL sensitivity experiments.

The MYJ turbulence closure scheme is a level 2.5, 1.5-order Turbulent Kinetic Energy (TKE) scheme that uses local vertical mixing in both the boundary layer and the free atmosphere (Mellor and Yamada, 1982). To diagnose PBL height, the MYJ scheme uses a critical TKE value of 0.001 $m^2 s^{-2}$, whereby values below this is are classed as the free atmosphere. Similar to the MYJ scheme, the Mellor-Yamada-Nakanishi-Niino is also a level 2.5 TKE scheme which uses the same basic TKE equations to complete turbulence closure. The difference between the MYJ and the MYNN schemes lies in the definition of the master length scale, which is important for the calculation of TKE. The MYNN scheme is much more complex than the MYJ, due to the explicit treatment of stability. Also, the MYNN scheme was verified using large-eddy simulations as this, unlike observations which were used for the MYJ scheme, prevents possible contamination by nonstationary mesoscale phenomena (Esau and Byrkjedal, 2007). Both TKE schemes performed better than the YSU scheme in the study by Krogsaeter et al. (2011), though notably the MYJ scheme has a tendency to produce overly shallow boundary layers (Sun and Ogura, 1980).

Finally, for comparison with the different sea breeze types, another baseline simulation is run without gradient winds.

ACPD
12, 15837–15881, 2012

3 Results

3.1 Single coast experiments

3.1.1 Baseline case (no gradient wind)

Away from the main influence of the sea breeze, the baseline case produces a boundary layer which reaches a maximum height of approximately 1550 m over the land surface (Fig. 6). This height is reached at approximately 14:00 UTC and lasts until 18:45 UTC where upon the boundary layer collapses at nightfall. Similarly, the background specific humidity steadily rises to 13.5 g kg^{-1}, reaching its peak approximately 15 min before the maximum height in the PBL (Fig. 6).

From approximately 02:00–09:00 UTC, a light shallow circulation is established over the coastline, indicative of a land breeze (Fig. 7). This breaks down and a very weak sea breeze with return flow emerges simultaneously, but it is not until after 12:00 UTC, that the sea breeze strength breaches the 1 m s^{-1} threshold and continues to intensify to 2.5 m s^{-1} by 18:00 UTC (Fig. 7).

The effect of the onset of the sea breeze on the PBL is to prevent entrainment and the consequent development of the convective boundary layer. Since the determination of the PBL height is, in this case, based on the bulk Richardson number, an increase in the strength of shear turbulence brought about by the formation of the sea breeze, suppresses the buoyancy instability over the land surface and therefore stabilizes the PBL. The arrival of the sea breeze also causes the specific humidity to drop (Fig. 6) in agreement with observations by Finkele (1998).

The overall depth of the sea breeze landward component is approximately 700 m, with a seaward return flow depth which is approximately twice the magnitude (Fig. 8). The depths found are consistent with observations presented by Simpson (1994) of sea breezes along the south coast of England. Ahead of the sea breeze onshore, a region of calm (<1 m s^{-1}) onshore flow of approximately the same length, but double the thickness of the sea breeze onshore flow, persists for the duration of the simulation.

ACPD
12, 15837–15881, 2012

This is indicative of continental air moving inland as the sea breeze advances (Miller et al., 2003). A vertically propagating wave develops, as shown in Fig. 8, and reaches a maximum height of 12 km by the end of the simulation (not shown). To our knowledge, there have been no observations of the vertically propagating wave in a sea breeze circulation, but they are frequently experienced and seen in simulations of mountain winds. Further study into this is beyond the scope of this paper since our primary focus remains in the offshore environment.

Applying the criteria defined by Arritt (1989) over the modelled sea, the sea breeze is more than capable of reaching over 250 km offshore. However, the scale of offshore advancement was sensitive to the speed threshold set. For example, increasing the threshold to 1.5 $m s^{-1}$ resulted in a reduction of approximately a third less offshore advancement. Even at a threshold of 2.5 $m s^{-1}$ the sea breeze still reaches 80 km offshore, confirming the potential for a sea breeze to affect a cell on an opposing coastline at scales typical of the Southern North Sea.

3.1.2 *Pure* sea breeze

For a *pure* type sea breeze with an offshore gradient wind of 2 $m s^{-1}$ the return flow component first establishes over the coast at 10:00 UTC, three hours before the development of the low level onshore flow, unlike the baseline case where they are coincident (not shown). The offshore extent becomes approximately equal to the baseline case for this gradient wind speed, extending to a maximum of 270 km offshore (Fig. 9). East of the seaward end of the sea breeze a calm zone (<1 $m s^{-1}$) extends a further 50 km offshore, so that by 19:00 UTC, the influence of the *pure* sea breeze extends across the entire offshore domain. The presence of a calm zone offshore has been observed in the Southern North Sea by Lapworth (2005) though only extend between 20–40 km during offshore gradient wind conditions.

Increasing the gradient offshore wind speed results in a delay of the establishment of the full sea breeze circulation. For example, increasing the offshore gradient wind from the baseline to 4 $m s^{-1}$ results in a delay of 2.5 h (Fig. 9). The onshore component

ACPD
12, 15837–15881, 2012

also weakens with increasing gradient wind speed to the extent that once the gradient speed becomes equal to 8 m s^{-1}, the onshore component does not breach the 1 m s^{-1} threshold used by Arritt (1989) and a sea breeze is not formed (compare Figs. 9 and 10).

The PBL height development is not substantially different from the baseline case with increasing wind speed, although the delay with the formation of the sea breeze results in the PBL at the coast becoming deeper before the onset (not shown). Increasing the gradient wind speed results in the formation of a front, denoted by a sharp rise in specific humidity at the onset of the sea breeze which is not present in the baseline case (not shown). This peak becomes more pronounced with increasing gradient wind speed until it reaches 8 m s^{-1} when the sea breeze is not formed.

Offshore, the horizontal extent of the sea breeze is sensitive to the strength of the gradient wind above 2 m s^{-1} to the degree that raising the gradient wind strength to 4 m s^{-1} reduces the maximum offshore extent to 20 km (Fig. 9). Calm zones (<1 m s^{-1}) extend a further 75 km offshore which are simulated in all experiments.

In context, a typical 100 m offshore wind turbine has a cut-in speed of 4 m s^{-1}, whereby at wind speeds below this threshold the turbine does not operate (Sinden, 2005). Therefore it is entirely possible for a *pure* sea breeze to have a negative influence on wind power production. Once above this threshold, the power produced is proportional to the cube of the wind speed, so at higher gradient wind speeds the sea breeze, acting in the opposite direction, can significantly reduce power output. In cases where the land-sea thermal contrast is of insufficient strength to produce a sea breeze, or where the offshore gradient wind is too strong, there is still a significant reduction in wind speed offshore which, for a period, is below the turbine cut-in speed (Fig. 11).

3.1.3 *Corkscrew* and *backdoor* sea breezes

As with the *pure* case, the formation of a *corkscrew* sea breeze in 2 m s^{-1} shore-parallel winds involved the establishment of the return flow circulation before the onset of the low-level onshore flow (not shown). This began to develop at 09:00 UTC, rather than

ACPD
12, 15837–15881, 2012

10:00 UTC, as with the *pure* case, supporting the theory that a *corkscrew* type sea breeze requires a weaker thermal contrast to initialize. The earlier onset time prevented the PBL height at the coast from reaching a height above 750 m before the arrival of the sea breeze (Fig. 12). Consequently the PBL height drop on arrival was not as sharp as with the equivalent *pure* case and by 16:00 UTC it had lowered to 300 m; the height of the PBL over the sea. This pattern was replicated for specific humidity (Fig. 12).

Increasing the strength of the shore-parallel gradient flow results in both an increase in the offshore extent and an earlier onset time, unlike the *pure* sea breeze which does not establish for offshore gradient wind speeds over 6 $m s^{-1}$ (Fig. 9 and 13). Also unlike the *pure* sea breeze, all gradient wind strengths produce a *corkscrew* sea breeze which has sufficient offshore extent to cross the entire offshore domain (Fig. 13).

The vertical thickness of the *corkscrew* sea breeze is approximately 900 m (Fig. 14) and does not deviate for increasing along-shore gradient flow. However, the depth of the return flow appears to increase substantially with increasing along-shore gradient wind speed, though the true degree is masked by rotation of the gradient winds by Coriolis acceleration.

Similarly, since the effect of Coriolis acceleration acting on a shore-parallel gradient wind orientated with the land surface to the right would be to generate onshore flow, it is not possible to calculate the offshore extent of a *backdoor* sea breeze using the method of Arritt (1989). However it can be noted that for an along-shore gradient wind speed of 2 $m s^{-1}$, the *backdoor* sea breeze begins approximately 30 km onshore. At this gradient wind speed, Coriolis acceleration is smaller and so the sea breeze is easily distinguished from the vertical zonal wind profile (Fig. 15).

Both the *corkscrew* and the *backdoor* sea breezes, produce stronger vector wind speeds offshore than at the coast unlike the *pure* sea breeze simulations (e.g. Fig. 16). The thickness of the *backdoor* sea breeze however approximated the *pure* case with a 700 m onshore flow and 1500 m return flow depth aloft (Fig. 15).

In summary, there are notable differences between the different types of sea breeze which warrant consideration by a forecaster. *Corkscrew* sea breezes are stronger and

ACPD
12, 15837–15881, 2012

thicker circulations than *pure* types and can be produced under gradient wind speeds which are too high for a *pure* type to establish. They also potentially have a much larger offshore extent and increase the wind speed offshore, unlike the *pure* type which acts to reduce the wind speed offshore. Similarly for *backdoor* types, though these are weaker and more difficult to distinguish from the background flow. Potentially, the offshore extents of the different sea breeze types and related calm zones could therefore affect offshore wind farms in the Southern North Sea. However the coastline of mainland Europe could modulate this and so we now move on to investigate the effect of an additional coastline in dual-coast simulations.

3.2 Dual-coast

3.2.1 Baseline cases (no gradient wind)

Similar to the previous single coastline example, a single simulation with no gradient winds superimposed was run this time for each boundary layer scheme. The simulation for the YSU scheme produced two symmetrical sea breezes on each coastline each with a peak offshore extent of 40 km at 17:00 UTC (Fig. 17). After this, the sea breeze retreated towards the coast until 19:00 UTC when no sea breeze was present offshore. The maximum strength of the onshore flow occurred approximately 30 km inland at 15:00 UTC with a speed of $4\,\mathrm{m\,s^{-1}}$. Eventually the onshore extent reached 60 km, until the sea breeze subsided after 17:00 UTC. Onshore flow inland remained present although it was not continuous from the coast after this time. The PBL height and 2 m specific humidity simulated were comparable to the single coast simulation, reaching maxima of 1550 m and $13.5\,\mathrm{g\,kg^{-1}}$, respectively, 150 km onshore from the western coast (not shown).

Both the MYJ and MYNN PBL schemes produce different baseline states (Fig. 17b and c). At 18:00 UTC both cases form pre-frontal waves of wavelength approximately 30 and 10 km for the MYJ (Fig. 17b) and MYNN (Fig. 17c) cases, respectively. Pre-frontal waves have both been observed and modelled elsewhere, with wavelengths

ACPD
12, 15837–15881, 2012

of approximately 10 km (Miller et al., 2003). These form in the late evening when the sea breeze interacts with a stabilizing nocturnal boundary layer inland. However, typically these dissipate quickly whereas the waves produced here traverse the model land domain. Furthermore, the MYJ scheme produces a much deeper PBL than the YSU baseline simulation, reaching 2300 m, and with 2 m specific humidity of 21 g kg^{-1} at 13:00 UTC, 150 km onshore (not shown). The MYNN scheme formed a shallower PBL than the YSU, reaching a maximum depth of 1300 m, however, it also simulated the highest 2 m specific humidities of 23 g kg^{-1}.

3.2.2 *Pure* sea breeze

Without the inclusion of Coriolis forcing in the simulation, increasing the strength of the offshore sea breeze gradient wind resulted in the western sea breeze retreating towards the sea. Indeed, for the YSU PBL scheme, the sea breeze did not reach the coastline at gradient wind speeds between 11–14 m s^{-1} (Fig. 19). The offshore extent of the sea breeze was insensitive to gradient wind speed below 11 m s^{-1}, reaching 40 km offshore.

With increasing gradient wind speed, both the MYJ and MYNN PBL schemes produce stronger 10 m wind speeds than the YSU scheme (Fig. 18). As a result, the maximum gradient wind speed that a *pure* sea breeze can form in is higher for the YSU PBL scheme with 13 m s^{-1}, compared to 10 m s^{-1} and 7 m s^{-1} for the MYJ and MYNN simulations, respectively. This is also a higher threshold than the previous single coast experiments using the YSU scheme. The confined sea in the dual-coast simulations is of insufficient length for the offshore gradient winds to fully adjust to the change in roughness length at the coast and is therefore more turbulent than with the single coast case. This means that the effective offshore gradient wind speed will be less than the single coast simulations and so the sea breeze will be able to form at higher gradient wind speeds for the dual-coast case.

The combination of the offshore calm zone (<1 m s^{-1}) and the sea breeze offshore extends to a greater distance with the YSU PBL, reaching 90 km compared with

ACPD
12, 15837–15881, 2012

maxima of 70 km for both the MYJ and MYNN schemes. However the offshore extents of all PBL schemes are comparible extending to 30 km, though the sensitivity of the MYNN PBL scheme is greater to increasing gradient wind speed.

The inclusion of Coriolis acceleration increases the sensitivity of the offshore extent of the *pure* sea breeze to increasing gradient wind speed (Fig. 19). The MYNN PBL scheme, in particular, does not simulate an onshore flow over the sea once Coriolis acceleration is included. With the YSU and MYJ schemes, the offshore extent does not become neglegable until gradient wind speeds above 6 $m s^{-1}$.

Similarly, the offshore calm zone is more sensitive to increasing gradient wind speed with the inclusion of Coriolis acceleration although this is not the case for the YSU PBL experiments. These extend to 70 km offshore until the gradient wind speed becomes equal to 10 $m s^{-1}$ and the sea breeze does not form. The maximum gradient wind speed that produces a sea breeze is similarly reduced for both the MYJ and MYNN schemes to 8 $m s^{-1}$ and 4 $m s^{-1}$, respectively.

In summary, the behaviour of the sea breeze offshore is strongly influenced by the choice of PBL scheme. The two TKE schemes tested simulate a *pure* sea breeze that is both shorter and more sensitive to gradient wind speed changes than the non-local YSU scheme. The MYNN PBL scheme in particular does not simulate a sea breeze in the offshore environment that meets the definition given by Arritt (1989)

Conversley, the inclusion of the second coastline allows the formation of a sea breeze in higher gradient wind speeds than the single coast simulations, though the length of both the offshore extent of the sea breeze and the calm zones are restricted by the inclusion of the second coastline. In context, though these are only idealized experiments, both the offshore calm zones and the *pure* sea breeze would influence any offshore wind farms, bringing the wind resource below the cut in threshold required to operate a turbine.

ACPD
12, 15837–15881, 2012

3.2.3 *Corkscrew* and *backdoor* cases

For a shore-parallel gradient wind without Coriolis acceleration, two symmetrical *corkscrew* and *backdoor* sea breezes are formed on each coastline for all gradient wind speeds (not shown). The inclusion of Coriolis acceleration however produces the asymmetry which the two sea breeze types to be distinguishable from each other (Fig. 20). This implies that Coriolis acceleration is responsible for the enhancing the regions of divergence and convergence when combined with the frictional differences between land and sea.

For all PBL schemes, increasing the strength of the along-shore gradient wind speed increases the extent and strength of the *corkscrew* sea breeze both onshore and offshore on the western coast, as per the single coast results (Fig. 20). This implies that the enhancement of the *corkscrew* sea breeze by creation of the region of divergence at coast becomes increasingly important with increasing gradient wind speed. The least sensitive PBL schemes to gradient wind speed changes are the YSU and MYJ schemes (Fig. 20b and c). As with the *pure* case, the MYNN scheme produces an offshore extent which is the smallest, reaching only 10 km for shore-parallel gradient wind speeds between 1–7 $m s^{-1}$. Above this speed, the *corkscrew* sea breeze becomes much more sensitive and rapidly increases so that by 17:00 UTC, a gradient wind speed of 18 $m s^{-1}$ is sufficient for the sea breeze to reach 90 km offshore (Fig. 20c). For both the YSU and MYJ schemes, the maximum offshore extent is again 90 km, however the increase is much more linear with increasing shore parallel gradient wind speed (Fig. 20a and b).

In contrast to the *corkscrew*, the *backdoor* sea breeze on the eastern coast has both the largest horizontal extent and strength at the lowest gradient wind speeds for all PBL schemes. There is little fluctuation in offshore extent until the point where the *corkscrew* sea breeze on the western coast prevents the formation of the *backdoor* sea breeze on the eastern. This varies for each PBL scheme. For the YSU scheme both the maximum offshore extent and the strength of the gradient wind speed required to

ACPD
12, 15837–15881, 2012

prevent sea breeze formation are the maximum between the different PBL schemes with values of 30 km and 15 $m s^{-1}$, respectively (Fig. 20a).

In summary, the factor responsible for the development of the asymmetries which distinguish the sea breeze types in shore parallel flow is Coriolis acceleration. For the *corkscrew* case, the creation of the region of divergence by Coriolis acceleration becomes increasingly important with increasing gradient wind speed to the degree that the *corkscrew* sea breeze restricts the development of the *backdoor* sea breeze on the eastern coastline. Also, for the wind speeds tested, increasing the strength of the along-shore gradient wind does not prevent the formation of a *backdoor* sea breeze, so this type is not restricted to low wind speeds, unlike the more intensely studied *pure* type.

3.2.4 SST variations

The results of varying the SST within a realistic range for June in the Southern North Sea did not have a significant effect on offshore advancement on any type of sea breeze (not shown). Arritt (1989) argued that if the SST was not sufficiently warm to form a convective boundary layer, then the sea breeze would not be affected. Referring back to the vertical profile in Fig. 5, it is confirmed that the profile would not become unstable if the surface temperatures were varied for the temperatures considered and so limited retardation of the sea breeze occurred.

4 Summary and conclusions

A series of idealized numerical experiments of different sea breeze types have been performed and the additional constraint of a second coastal boundary has been tested. Of particular interest are the sea breeze characteristics and impact offshore, as extensive offshore wind farm development is currently underway in, for example, the

ACPD
12, 15837–15881, 2012

Southern North Sea. Sensitivity tests have also been performed regarding PBL physics schemes and realistic variations in sea surface skin temperature.

Principally, it is found that consideration must be given to the sea breeze type, if accurate prediction of the sea breeze characteristics is to be achieved. This is especially important offshore, as both *corkscrew* and *backdoor* types produce higher wind speeds here than at the coast. In contrast to this, the *pure* sea breeze causes a reduction in wind speed offshore relative to the coastline.

The inclusion of the second coastline, more realistically reepresenting the Southern North Sea, causes the formation of calm zones ($<1\,m\,s^{-1}$) which frequently span a large proportion of the modelled water surface. Also, the *pure* sea breeze is able to form in higher gradient wind speeds than the single coast case. The smaller water surface does not allow the airflow to fully adjust before arrival at the second coastal boundary and so the airflow here is more turbulent, reducing the effective wind speed. Both the presence of the second coastline and the sea breeze type considered potentially have significant implications for offshore wind farms. This result is not particularly sensitive to realistic SST variations, however, there are important differences with regard to the PBL scheme used. In particular, the MYNN scheme simulates much weaker *pure* sea breezes offshore, extending to less than 10 km for the majority of simulations, yet the extent of the simulated calm zone is comparable to other PBL schemes.

For all of the shore-parallel gradient wind simulations, a *corkscrew* sea breeze was formed on the western coast, and was intensified offshore relative to the baseline case (no gradient wind). Increasing the gradient wind speed further extended the *corkscrew* sea breeze offshore until it reached the opposite coastline. This occurred for all PBL schemes.

Since a *corkscrew* type sea breeze occurred on the opposite coastline to the *backdoor* sea breeze, the offshore extent of the *backdoor* sea breeze was restricted by the *corkscrew*. Consequently, the circulation was restricted to its own coastline. This, however, only occurred when Coriolis was enabled. Without Coriolis rotation, both coastlines produced identical sea breezes, and the distinct *corkscrew* and *backdoor* types

ACPD
12, 15837–15881, 2012

were not generated. This implies that Coriolis acceleration plays an important role in forming the different sea breeze types, and that in particular, the divergence associated with the *corkscrew* sea breeze becomes increasingly important with increasing gradient wind speed.

Whilst these results are purely idealized, they present an indication to the forecaster of the sea breeze dependence on both prognostic variables and physical model settings. Further research will be carried out through the modelling of real events coupled with verification of the results against measurements from offshore wind farms in the Southern North Sea to help determine the relative accuracies of the PBL schemes.

Acknowledgements. The authors would like to acknowledge both the National Environmental Research Council (NERC) and Weatherquest Ltd. for providing the funding to make this research possible.

References

Abbs, D. J. and Physick, W. L.: Sea-breeze observations and modelling: a review, Aust. Meteorol. Mag., 41, 7–19, 1992. 15839

Arritt, R. W.: Numerical modelling of the offshore extent of sea breezes, Q. J. Roy. Meteorol. Soc., 115, 547–570, 1989. 15840, 15841, 15844, 15847, 15848, 15849, 15852, 15854

Azorin-Molina, C. and Chen, D.: A climatological study of the influence of synoptic-scale flows on sea breeze evolution in the Bay of Alicante (Spain), Theor. Appl. Climatol., 96, 249–260, doi:10.1007/s00704-008-0028-2, 2009. 15840

Azorin-Molina, C., Chen, D., Tijim, S., and Baldi, M.: A multi-year study of sea breezes in a Mediterranean coastal site: Alicante (Spain), Int. J. Climatol., 31, 468–486, 2011a. 15839

Azorin-Molina, C., Tijm, S., and Chen, D.: Development of selection algorithms and databases for sea breeze studies, Theor. Appl. Climatol., 106, 531–546, doi:10.1007/s00704-011-0454-4, 2011b. 15840

Bianco, L., Tomassetti, B., Coppola, E., Fracassi, A., Verdecchia, M., and Visconti, G.: Thermally driven circulation in a region of complex topography: comparison of wind-profiling radar measurements and MM5 numerical predictions, Ann. Geophys., 24, 1537–1549, doi:10.5194/angeo-24-1537-2006, 2006. 15839

ACPD

12, 15837–15881, 2012

Borge, R., Alexandrov, V., José del Vas, J., Lumbreras, J., and Rodríguez, E.: A comprehensive sensitivity analysis of the WRF model for air quality applications over the Iberian Peninsula, Atmos. Environ., 42, 8560–8574, available at: http://www.sciencedirect.com/science/article/B6VH3-4TDVMKT-1/%2/5ba8a6c0e2b5913542b57f92e7f14806, 2008. 15839

Brian, G., Peter, C., and Bryony, M.: The Boscastle flood: meteorological analysis of the conditions leading to flooding on 16 August 2004, Weather, 60, 230–235, doi:10.1256/wea.71.05, 2005. 15839

Challa, V. S., Indracanti, J., Rabarison, M. K., Patrick, C., Baham, J. M., Young, J., Hughes, R., Hardy, M. G., Swanier, S. J., and Yerramilli, A.: A simulation study of mesoscale coastal circulations in Mississippi Gulf coast, Atmos. Res., 91, 9–25, doi:10.1016/j.atmosres.2008.05.004, 2009. 15839, 15845

Clarke, R. H.: Sea-breezes and waves: the "Kalgoorlie sea-breeze" and the "Goondiwindi breeze", Aust. Meteorol. Mag., 37, 99–107, available at: http://www.scopus.com/inward/record.url?eid=2-s2.0-0024794650%&partnerID=40, 1989. 15839

Clarke, R. H., Smith, R. K., and Reid, D. G.: The morning glory of the Gulf of Carpentaria: an atmospheric undular bore, Mon. Weather Rev., 109, 1726–1750, available at: http://www.scopus.com/inward/record.url?eid=2-s2.0-0019715999%&partnerID=40, 1981. 15839

Cleantech: Jefferies CleanTech Review, http://energy.wesrch.com/page-summary-pdf-TR1AU1TUOWTVP-jefferies-cleantech-review-26, last access: 15 June 2012, 2010. 15864

Crosman, E. T. and Horel, J. D.: Sea and lake breezes: a review of numerical studies, Bound.-Lay. Meteorol., 137, 1–29, doi:10.1007/s10546-010-9517-9, 2010. 15839, 15840, 15841, 15843, 15844

Esau, I. and Byrkjedal, Y.: Application of a Large-Eddy simulation database to optimisation of first-order closures for neutral and stably stratified boundary layers, Bound.-Lay. Meteorol., 125, 207–225, doi:10.1007/s10546-007-9213-6, 2007. 15845

Fernández-Camacho, R., Rodríguez, S., de la Rosa, J., Sánchez de la Campa, A. M., Viana, M., Alastuey, A., and Querol, X.: Ultrafine particle formation in the inland sea breeze airflow in Southwest Europe, Atmos. Chem. Phys., 10, 9615–9630, doi:10.5194/acp-10-9615-2010, 2010. 15839

Finkele, K.: Inland and offshore propagation speeds of a sea breeze from simulations and measurements, Bound.-Lay. Meteorol., 87, 307–329, 1998. 15840, 15841, 15846

ACPD
12, 15837–15881, 2012

Furberg, M., Steyn, D. G., and Baldi, M.: The climatology of sea breezes on Sardinia, Int. J. Climatol., 22, 917–932, doi:10.1002/joc.780, 2002. 15839
Hoddinott, M. H. O.: Failure of the sea-breeze in Chester during a hot spell, Weather, 64, p. 310, doi:10.1002/wea.491, 2009. 15840
Hong, S. Y., Noh, Y., and Dudhia, J.: A new vertical diffusion package with an explicit treatment of entrainment processes, Mon. Weather Rev., 134, 2318–2341, 2006. 15844
Krogsaeter, O., Reuder, J., and Hauge, G.: WRF and the marine planetary boundary layer, available at: http://www.mmm.ucar.edu/wrf/users/workshops/WS2011/Extended%20Abstracts%202011/P18_Krogsaeter_ExtendedAbstract_11.pdf, 12th Annual WRF users' workshop, National Center for Atmospheric Research, 20–24 June 2011. 15845
Lapworth, A.: The diurnal variation of the marine surface wind in an offshore flow, Q. J. Roy. Meteorol. Soc., 131, 2367–2387, doi:10.1256/qj.04.161, 2005. 15847
Lee, S.-H., Kim, S.-W., Angevine, W. M., Bianco, L., McKeen, S. A., Senff, C. J., Trainer, M., Tucker, S. C., and Zamora, R. J.: Evaluation of urban surface parameterizations in the WRF model using measurements during the Texas Air Quality Study 2006 field campaign, Atmos. Chem. Phys., 11, 2127–2143, doi:10.5194/acp-11-2127-2011, 2011. 15839
Mellor, G. L. and Yamada, T.: Development of a turbulence closure model for geophysical fluid problems, Rev. Geophys. Space Ge, 20, 851–875, 1982. 15845
Miller, S. T. K., Keim, B. D., Talbot, R. W., and Mao, H.: Sea breeze: structure, forecasting and impacts, Rev. Geophys., 41, 1011, doi:10.1029/2003RG000124, 2003. 15839, 15840, 15847, 15851, 15862
Papanastasiou, D., Melas, D., and Lissaridis, I.: Study of wind field under sea breeze conditions; an application of WRF model, Atmos. Res., 98, 102–117, doi:10.1016/j.atmosres.2010.06.005, 2010. 15839
RenewableUK: 10 facts about UK offshore wind, http://www.bwea.com/offshore/index.html, last access: 15 June 2012 15842
Savijarvi, H. and Alestalo, M.: The Sea breeze over a lake or gulf as the function of the prevailing flow, Beitraege zur Physik der Atmosphaere, 61, 98–104, 1988. 15839, 15842
Simpson, J. E.: Sea Breeze and Local Winds, Cambridge University Press, 1994. 15839, 15843, 15846
Sinden, G.: Wind Power and the UK Wind Resource, Tech. rep., Environmental Change Institute, University of Oxford, 2005. 15848

ACPD
12, 15837–15881, 2012

Skamarock, W. C. and Klemp, J. B.: A time-split nonhydrostatic atmospheric model for weather research and forecasting applications, J. Comput. Phys., 227, 3465–3485, available at: http://www.sciencedirect.com/science/article/B6WHY-4N2TS5M-1/%2/40f5f823c4917711bcebb65d6fb3ccb7, 2008. 15843

Sun, W.-Y. and Ogura, Y.: Modeling the evolution of the convective planetary boundary layer, J. Atmos. Sci., 37, 1558–1572, 1980. 15845

Tsunematsu, N., Iwai, H., Murayama, Y., Yasui, M., and Mizutani, K.: The formation of sharp multi-layered wind structure over tokyo associated with sea-breeze circulation, SOLA – Scientific Online Letters on the Atmosphere, 5, 1–4, available at: https://www.jstage.jst.go.jp/article/sola/5/0/5_0_1/_article, 2009. 15839

ACPD

12, 15837–15881, 2012

Table 1. WRF model and physics specifications used for the single coast baseline experiments.

WRF Setting and physics options	Value
Horizontal resolution (km)	3
Long wave physics	RRTM
Short wave physics	Monin-Obukhov similarity
Model top (hPa)	50
Ground physics	Noah land surface
PBL scheme	YSU
Vertical levels	35
Cumulus scheme	None
Microphysics	WSM-3-class
Coriolis (s^{-1})	1.15×10^{-4}

ACPD
12, 15837–15881, 2012

Table 2. Sensitivity tests for the dual-coast experiments. Note that WRF has two MYNN PBL schemes available. In all experiments the MYNN level 2.5 scheme is used.

Parameter	Sensitivity test
u-wind (ms^{-1})	0 to 20, steps of 1
v-wind (ms^{-1})	−20 to 20, steps of 1
SST (K)	280 to 290, steps of 1
PBL Schemes	YSU, MYNN (level 2.5), MYJ
Coriolis (s^{-1})	0, 1.15×10^{-4}

ACPD
12, 15837–15881, 2012

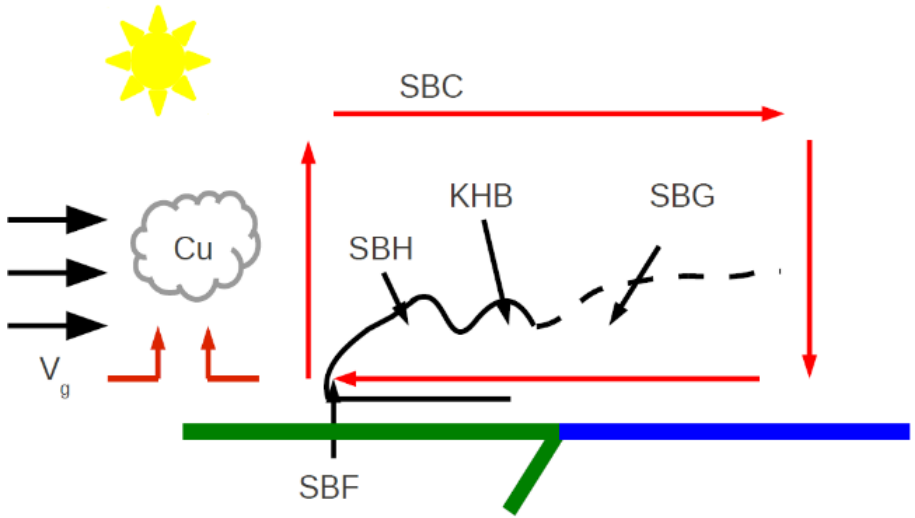

Fig. 1. Classical representation of a *pure* sea breeze adapted from Miller et al. (2003). The labelled features are the Sea Breeze Circulation (SBC), Sea Breeze Head (SBH), Cumulus (Cu), Sea Breeze Gravity Current (SBG), Gradient wind (V_g), Sea Breeze Front (SBF) and Kelvin-Helmholtz Billows (KHB).

ACPD
12, 15837–15881, 2012

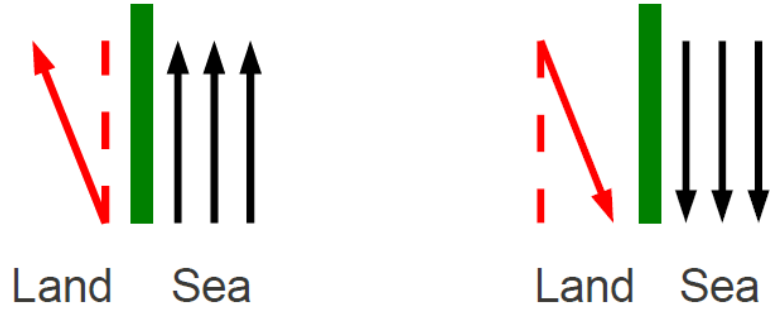

Fig. 2. Plan views of *corkscrew* (left) and *backdoor* (right) sea breeze generating scenarios depicting the effect of shore parallel gradient winds on a coastline (green). The black arrows depict the unaltered gradient wind direction. The red arrows portray frictional effects on the gradient flow at the coastline.

ACPD
12, 15837–15881, 2012

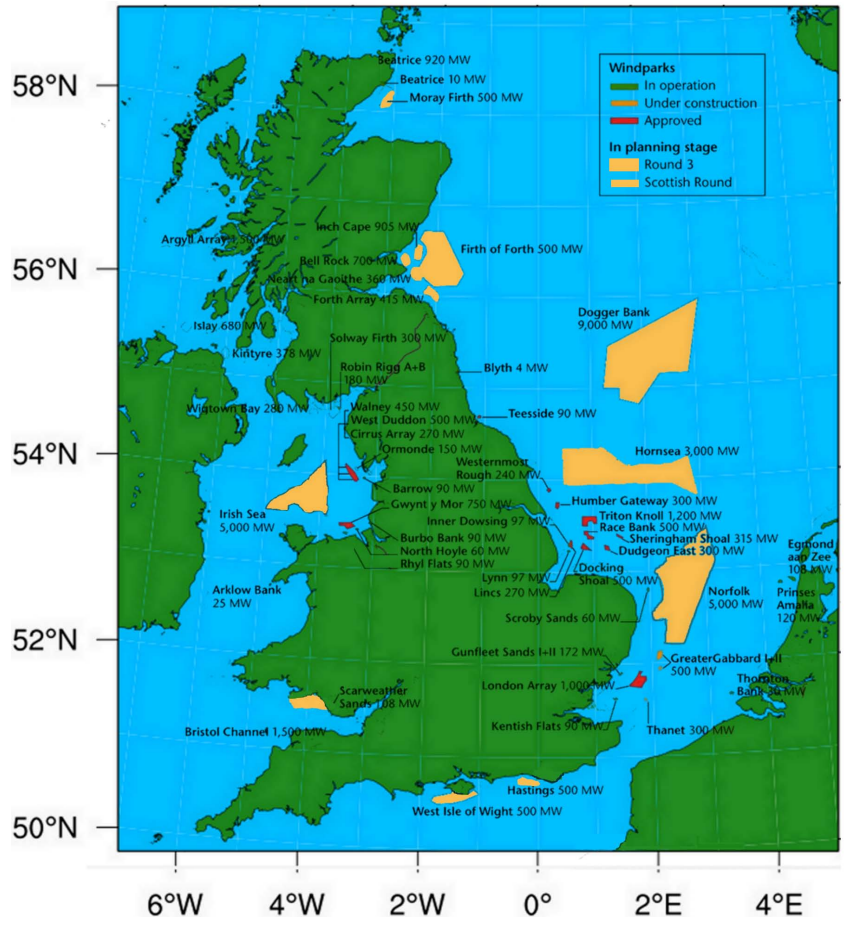

Fig. 3. The locations of constructed or planned offshore wind farms in the UK (Map after Cleantech, 2010).

ACPD
12, 15837–15881, 2012

Sensitivity simulations of sea breeze types

C. J. Steele et al.

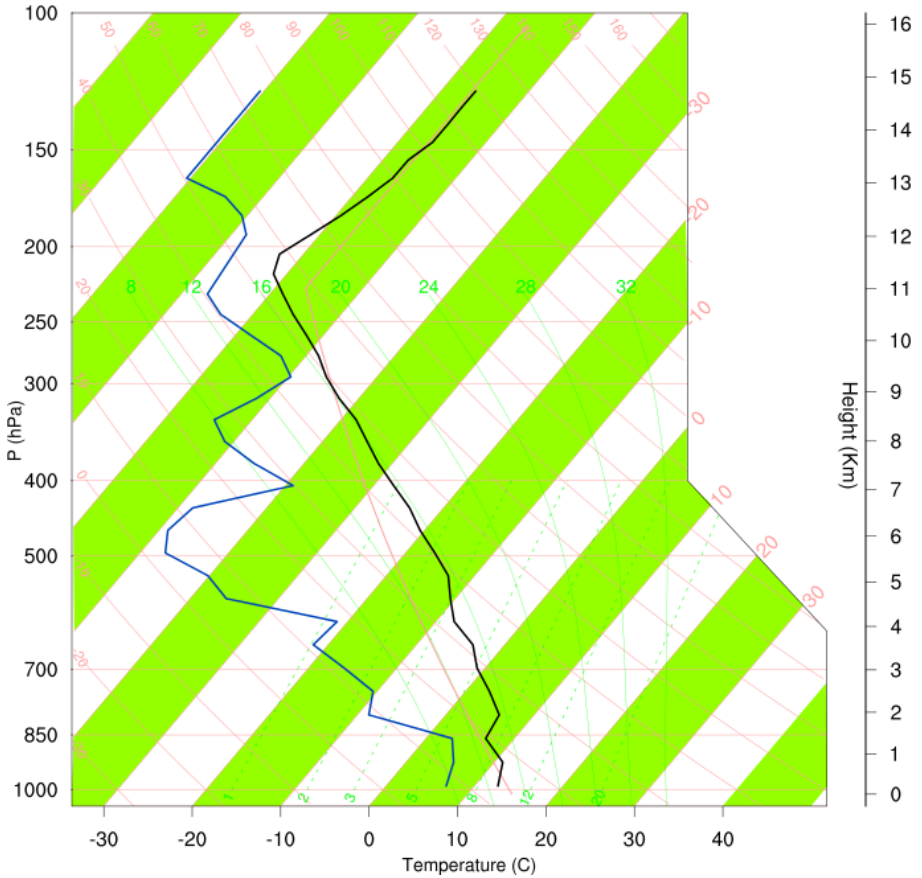

Fig. 4. The initialization vertical dry bulb and dewpoint temperature profile at the model coastline. The profile is observed at Herstmonceux station at midnight on the 3 June 2006.

ACPD
12, 15837–15881, 2012

Sensitivity simulations of sea breeze types

C. J. Steele et al.

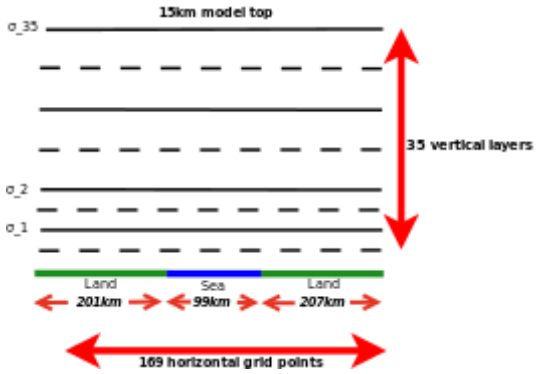

Fig. 5. Model configuration for dual coast experiments. Dashed lines indicate half levels on the Arakawa C-staggered grid used in the WRF model.

ACPD
12, 15837–15881, 2012

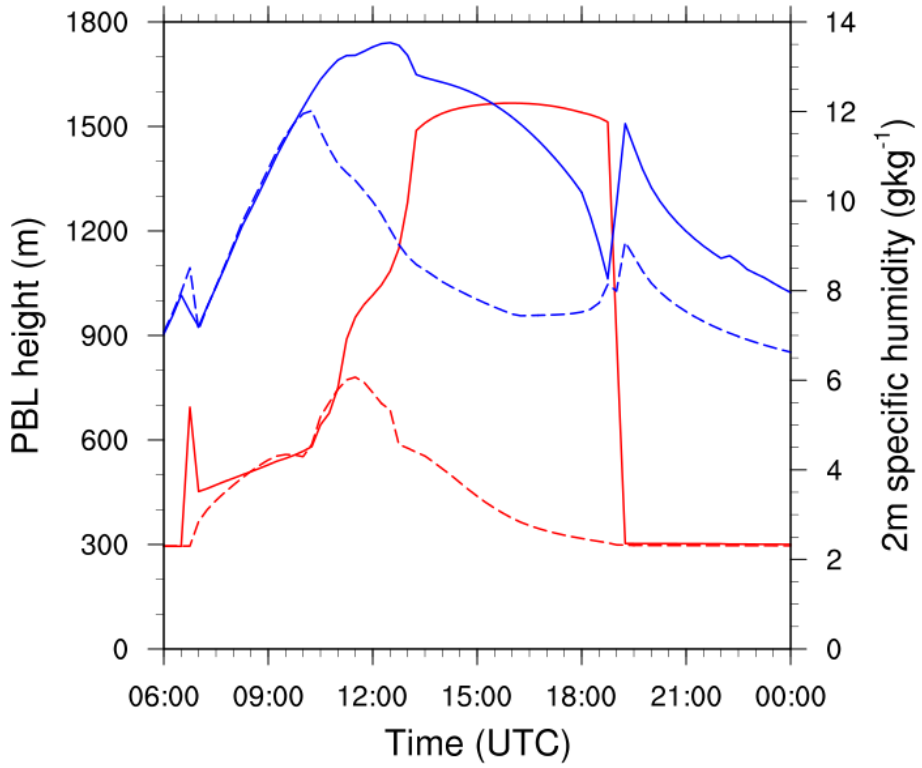

Fig. 6. Daytime evolution of PBL height (red) and 2 m specific humidity (blue) for the baseline single coast simulation. Solid lines indicate values 150 km onshore and dashed lines are at the coastline.

ACPD
12, 15837–15881, 2012

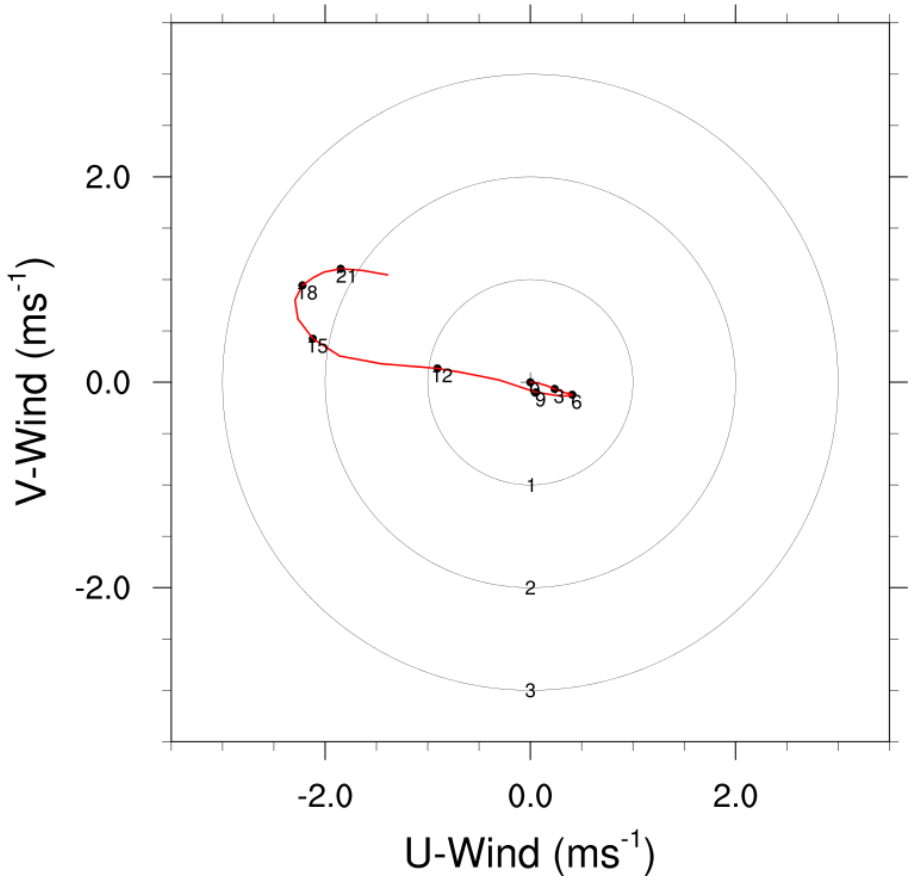

Fig. 7. Hodograph of the baseline simulation showing both a land and a sea breeze at the coastline using 10 m winds. Numbers labelled on the curve represent time in UTC and concentric circles portray the magnitude of the 10 m vector wind.

ACPD
12, 15837–15881, 2012

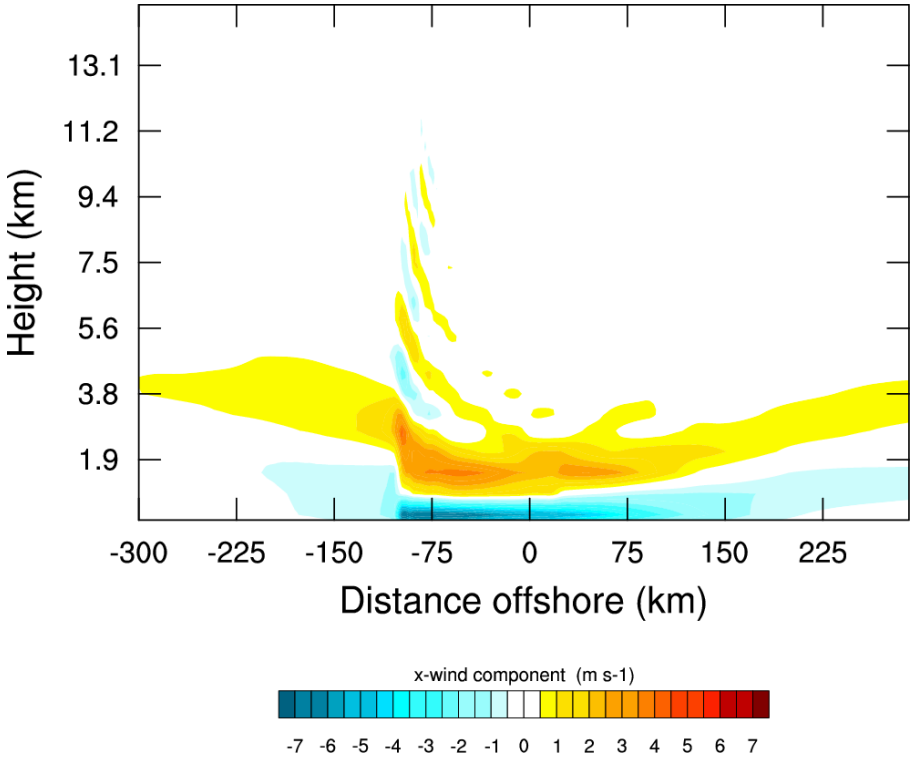

Fig. 8. The u-wind component (ms^{-1}) of a mature sea breeze at 19:00 UTC for the baseline case.

ACPD
12, 15837–15881, 2012

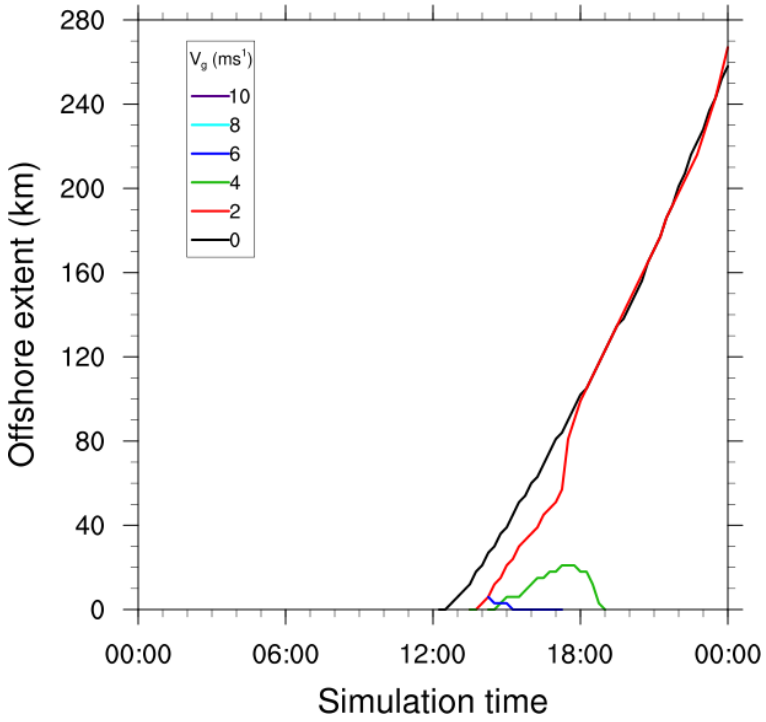

Fig. 9. Sensitivity of onset time and offshore extent of a *pure* sea breeze to the strength of the offshore gradient flow (V_g).

ACPD
12, 15837–15881, 2012

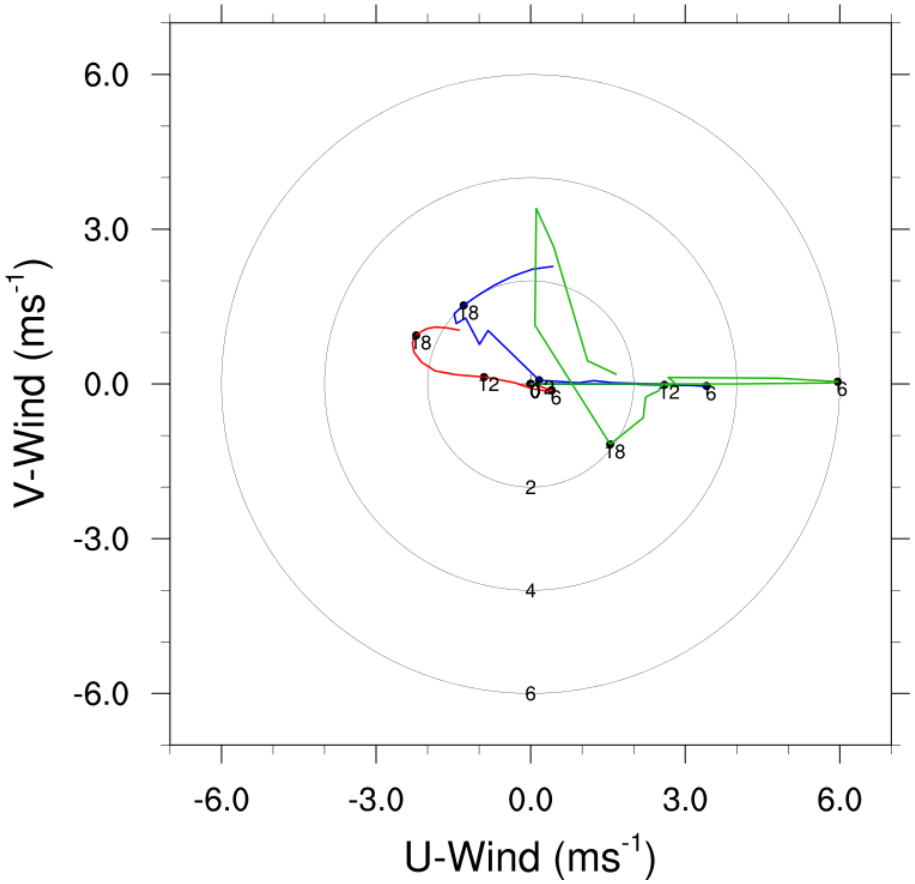

Fig. 10. Coastal 10 m hodograph for the baseline (red), 4 m s^{-1} (blue) and 8 m s^{-1} (green) offshore gradient winds. Numbers indicate simulation time in UTC and conccentric circles indicate the magnitude of the 10 m wind speed vector.

ACPD
12, 15837–15881, 2012

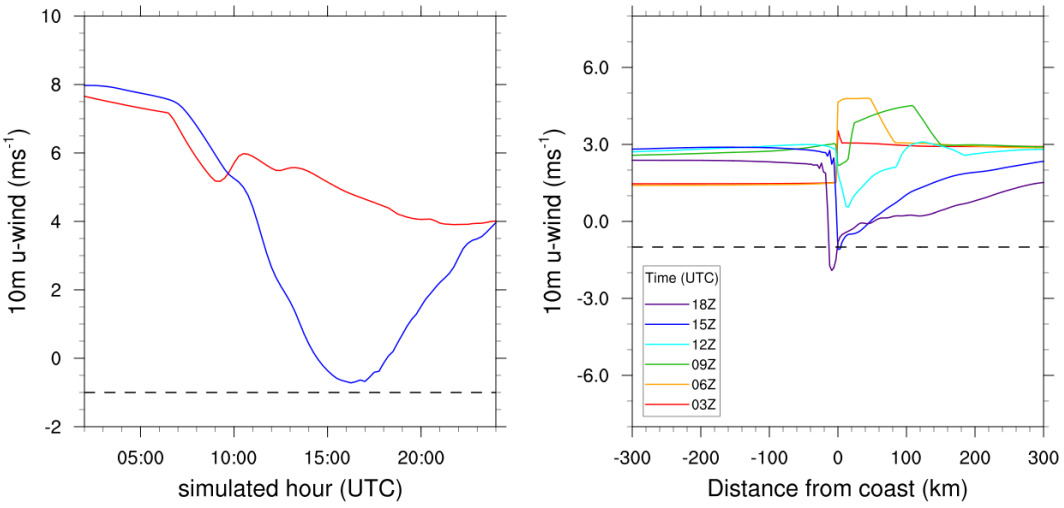

Fig. 11. (a) 10 m u-wind speed for locations on the coastline (red) and 30 km offshore (blue) for a *pure* sea breeze simulated with 8 m s^{-1} offshore gradient wind. **(b)** 10 m vector wind speed accross the model domain at 03:00 (red), 06:00 (orange), 09:00 (green), 12:00 (cyan), 15:00 (blue) and 18:00 (purple) UTC. The dashed line represents the 1 m s^{-1} offshore wind speed threshold required for diagnosing a sea breeze.

ACPD
12, 15837–15881, 2012

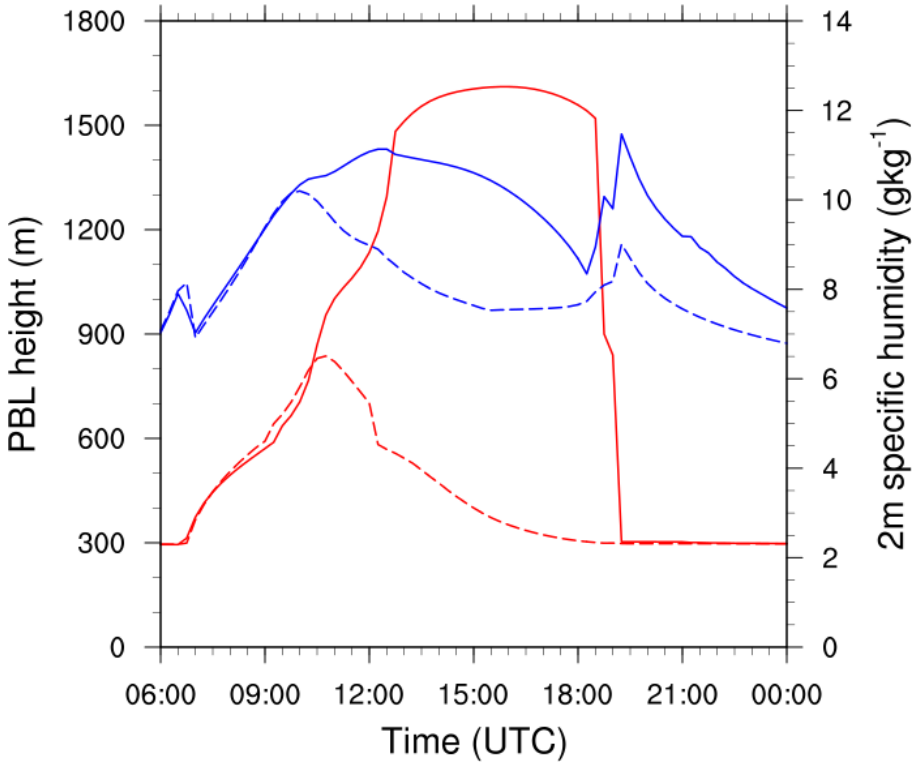

Fig. 12. 2 m specific humidity (blue) and PBL height (red) for a *corkscrew* simulation with 2 m s^{-1} along-shore gradient winds. Solid and dashed lines represent values at 150 km onshore and at the coast, respectively.

ACPD
12, 15837–15881, 2012

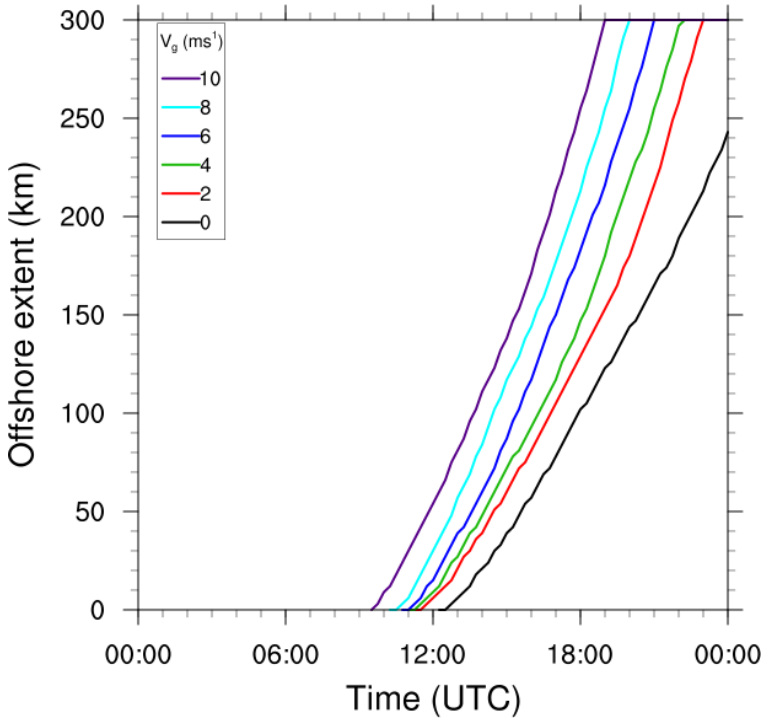

Fig. 13. Sensitivity of the onset time and of the offshore extent of the *corkscrew* sea breeze to the strength of the shore-parallel gradient flow.

ACPD
12, 15837–15881, 2012

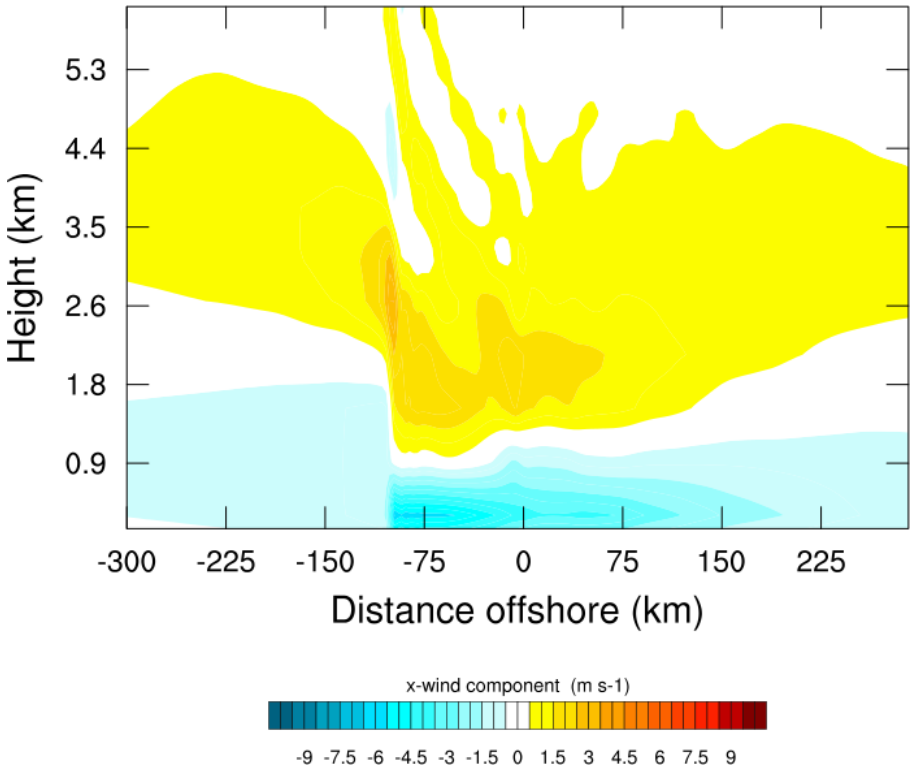

Fig. 14. Cross-section of a mature *corkscrew* sea breeze at 19:00 UTC developing in 2 m s^{-1} along shore gradient flow for the single coastline case.

ACPD
12, 15837–15881, 2012

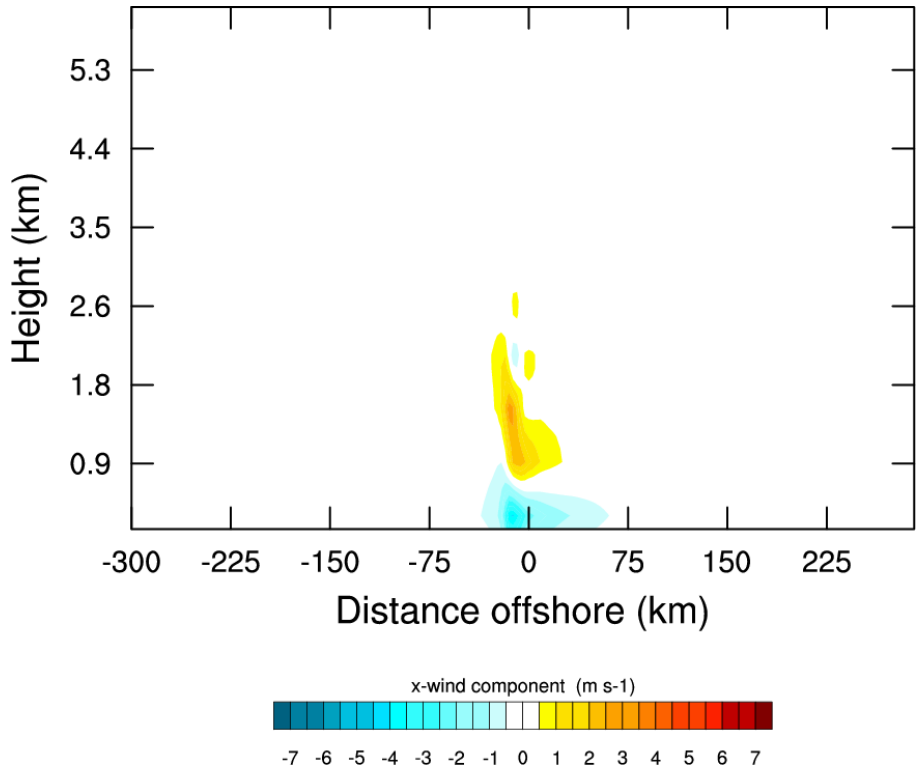

Fig. 15. Cross-section of a *backdoor* type sea breeze at 12:00 UTC generated with shore-parallel gradient winds of 2 m s^{-1} for the single coast case.

ACPD
12, 15837–15881, 2012

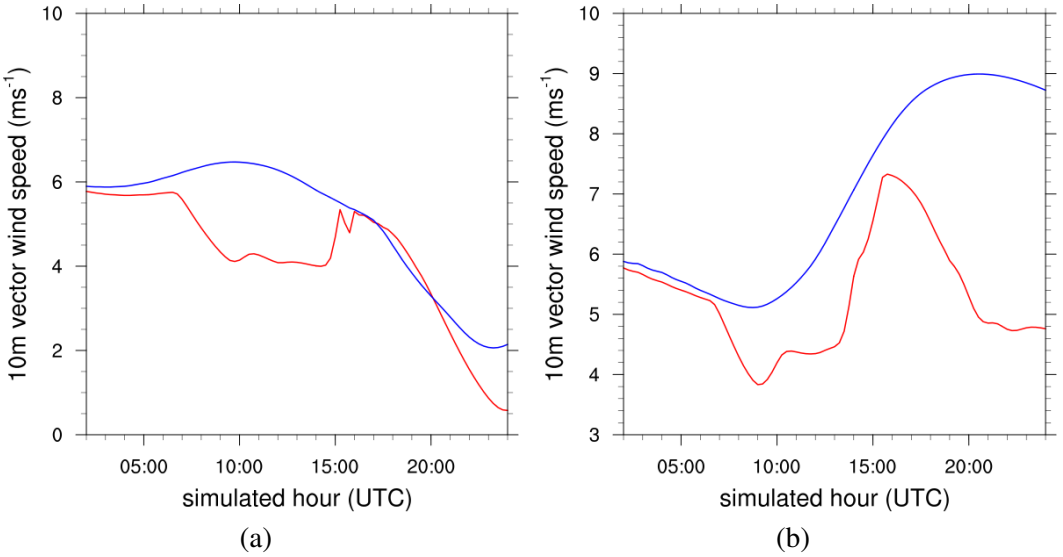

Fig. 16. The evolution of 10 m vector wind speed for *backdoor* **(a)** and *corkscrew* **(b)** sea breezes at the coast (red) and 30 km offshore (blue). Shore-parallel gradient winds for both cases are 6 m s^{-1}.

ACPD
12, 15837–15881, 2012

Sensitivity simulations of sea breeze types

C. J. Steele et al.

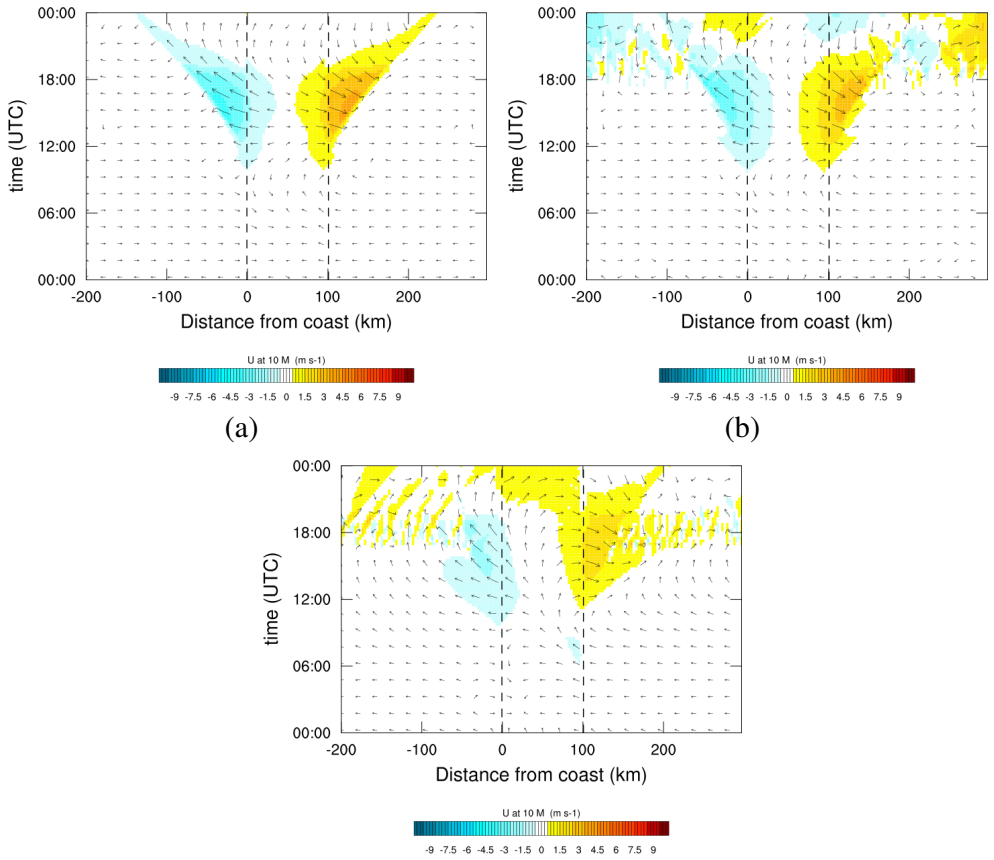

Fig. 17. Baseline windfield cases (no gradient wind) for dual-coast simulations using **(a)** YSU, **(b)** MYJ and **(c)** MYNN boundary layer schemes. Dashed lines represent each coastal boundary and distances are expressed as seaward from the western coastline.

ACPD
12, 15837–15881, 2012

Sensitivity simulations of sea breeze types

C. J. Steele et al.

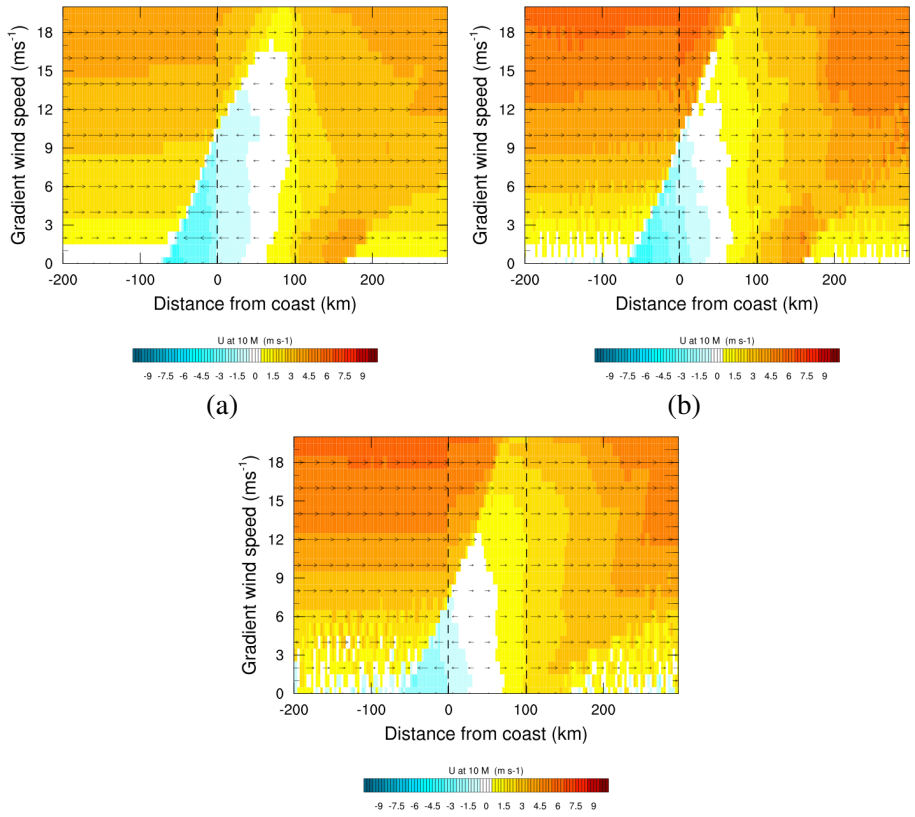

Fig. 18. Variations of the 10 m u-wind component (color) and vector wind speeds (arrows) with increasing west-east gradient wind strength at 17:00 UTC using the **(a)** YSU, **(b)** MYJ and **(c)** MYNN PBL schemes without Coriolis acceleration. Distances are measured from the western coastal boundary with each being depicted by the dashed lines.

ACPD
12, 15837–15881, 2012

Sensitivity simulations of sea breeze types

C. J. Steele et al.

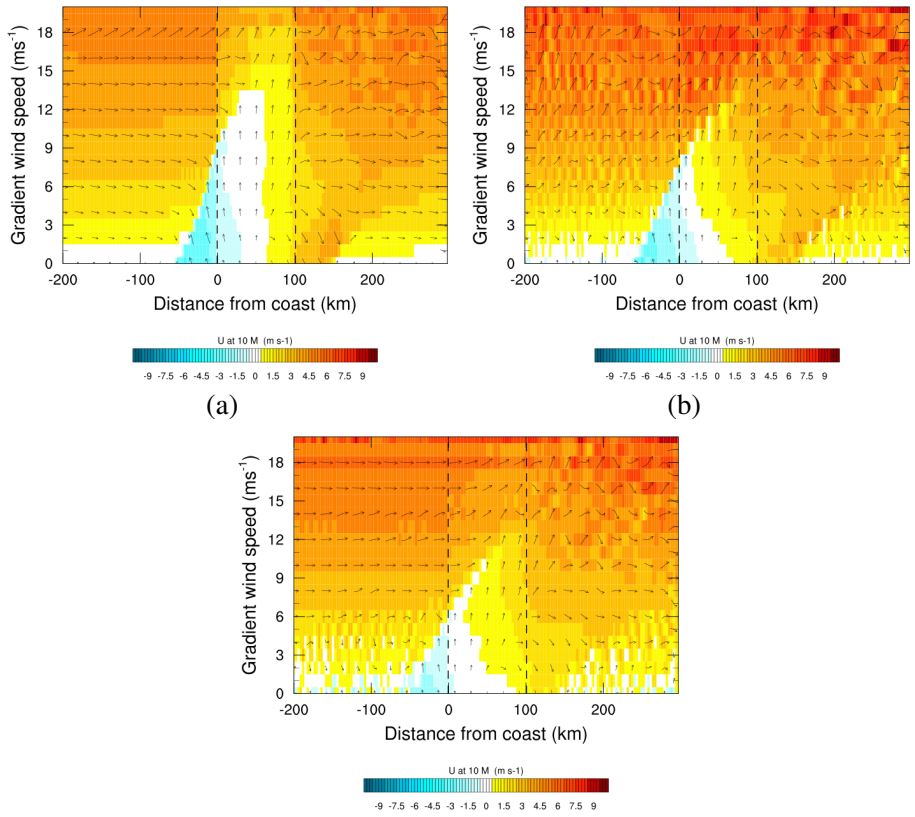

Fig. 19. Variations of the 10 m u-wind component (color) and vector wind speeds (arrows) with increasing west-east gradient wind strength at 17:00 UTC using the **(a)** YSU, **(b)** MYJ and **(c)** MYNN PBL schemes with Coriolis acceleration. Distances are measured from the western coastal boundary with each being depicted by the dashed lines.

ACPD
12, 15837–15881, 2012

Sensitivity simulations of sea breeze types

C. J. Steele et al.

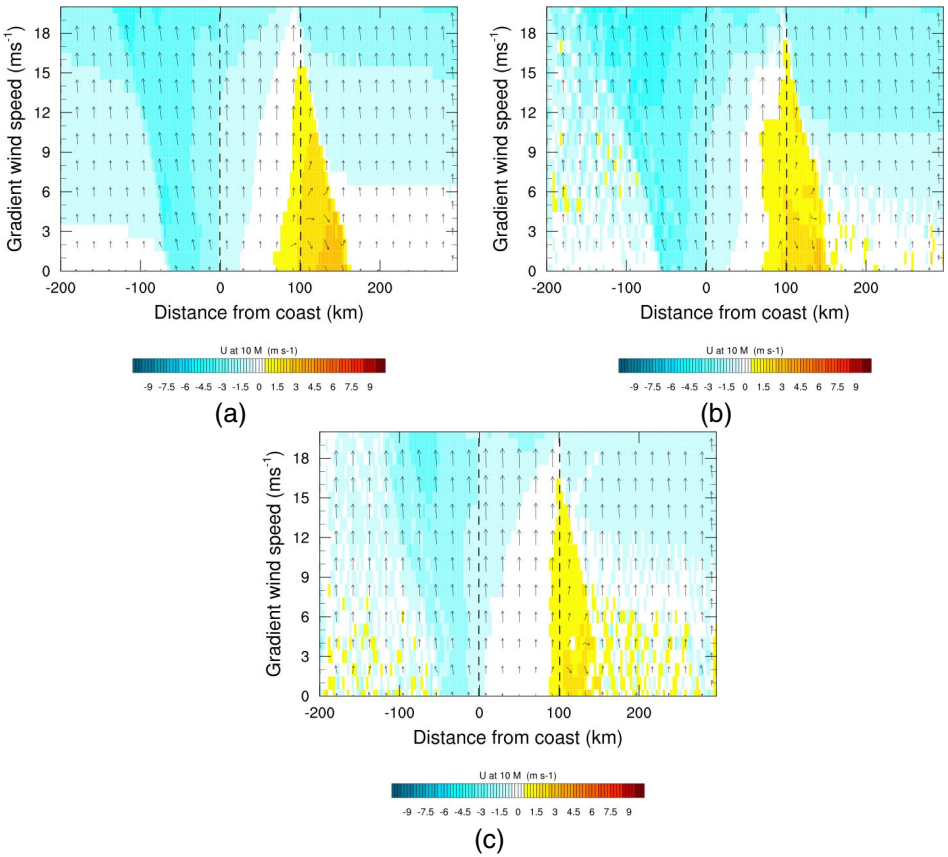

Fig. 20. Variations of 10 m u-wind component (colour) with 10 m wind vectors (arrows) for increasing south-north gradient winds at 17:00 UTC using the **(a)** YSU, **(b)** MYJ and **(c)** MYNN PBL schemes. Coriolis acceleration is enabled for a latitude of 52° and distances are measured from the western coast.

ACPD
12, 15837–15881, 2012

Sensitivity simulations of sea breeze types

C. J. Steele et al.